Chapter 3

Trapping antiprotons in an ion trap

A small number of keV protons (Fig. 3.1) and antiprotons (Fig. 3.2) were briefly trapped during feasibility tests [7,9]. With improved apparatus and technique (5.9 MeV LEAR beam instead of 21 MeV, vacuum improvement, energy ramp technique to avoid saturation in detection system), and more beam time to check the system routinely, we are able to trap antiprotons 100 times more efficiently and hold them indefinitely.

A simple diagram of the ion trap which consists a load endcap (the left cylinder), a ring (the central cylinder) and a dump endcap (the right cylinder) is shown in Fig. 3.1(a). Antiprotons approach from the left along the magnet field direction and are captured. They leave the trap toward the right and are detected. In a new mode of operation, the beam from LEAR is extracted in fast extraction which delivers a 300 ns pulse of antiprotons containing up to 3×10^8 particles. Because 3 keV particles transit the trap in less than 0.5 μs, only one particle would be present in the trap in slow extraction even if the beam is continuous with a rate of 2000 kHz. The fast extraction allows many more particles within the trap during the short pulse so that they can be trapped efficiently.

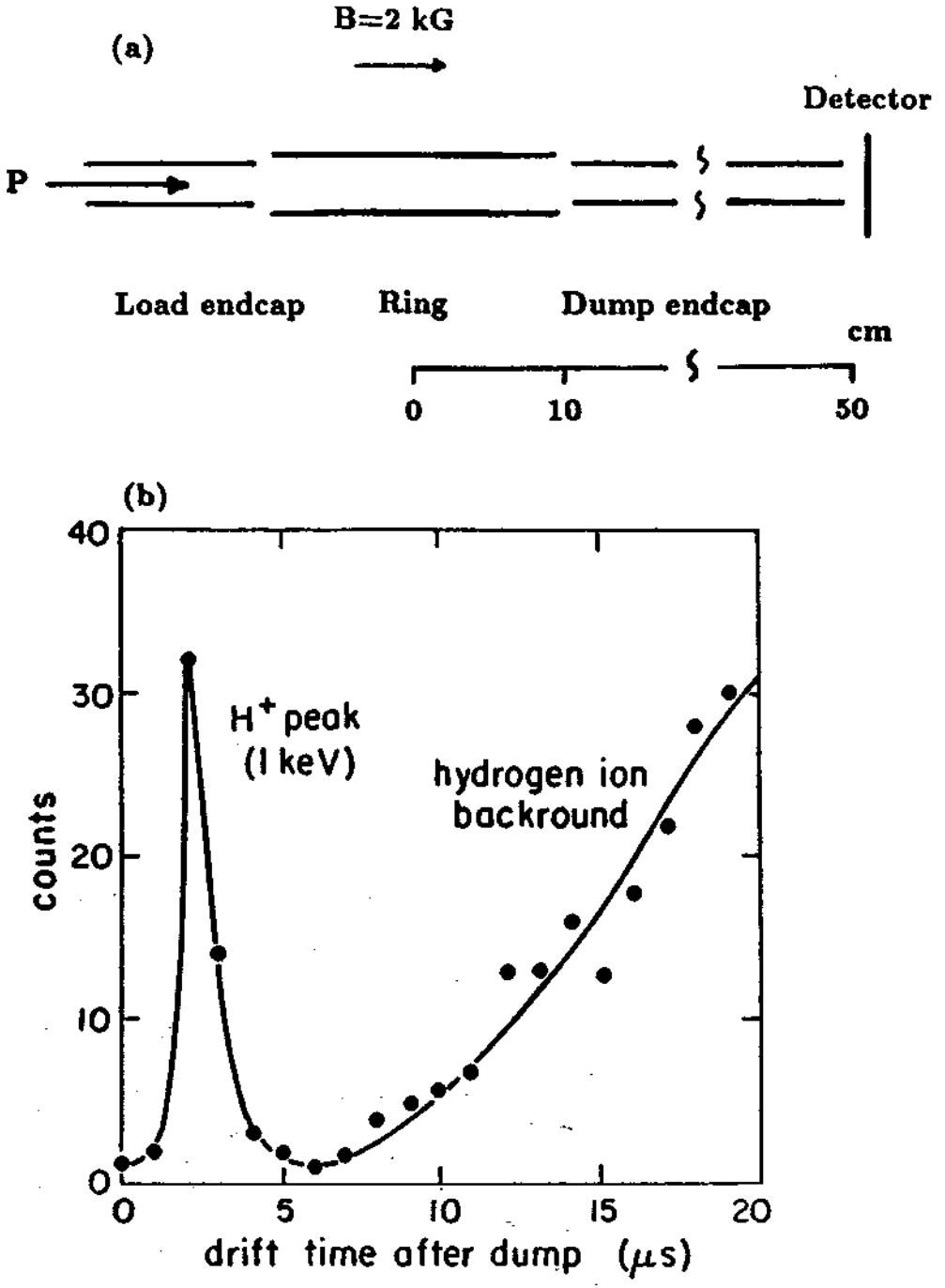

Figure 3.1: First direct trapping of keV protons.(a) Ion trap. (b) Particle counts.

We rely on the magnetic field to provide radial confinement. A 6 Tesla magnetic field is used to confine antiprotons radially when their radial energy $E_r = mv_r^2/2$ is not too large. From the formula $mv_r^2/r_c = ev_rB$, we have the radius of the cyclotron motion $r_c = mv_r/eB$, or,

$$r_c = (\sqrt{2mE_r})/eB. \tag{3.1}$$

The radius can also be written as

$$r_c(mm) = 2.4 \times 10^{-2}\sqrt{E(eV)}. \tag{3.2}$$

For example, the cyclotron radius for antiproton cyclotron energy of 25 eV (velocity is 7×10^4 m/sec) is 0.12 mm. It is 0.6 mm for radial energy of 0.63 keV (or velocity of 3.5×10^5m/sec). The trap radius is 6 mm which corresponds to a cyclotron energy of 63 keV.

We trap the keV particles directly, without slowing them, by applying kilovolt potentials to the trapping electrodes for axial confinement after the particles have entered the trap. The kilovolt potentials must be applied quickly compared to the transit time of the particles through the trap. We have been able to apply 3kV potentials in about 20 ns using krytrons as described in Chapter 4 [53]. We describe briefly the first trapping of protons and antiprotons in the next two sections. Then the greatly improved antiproton trapping experiment will be discussed.

3.1 First direct trapping of keV protons

To investigate the trapping process, we obtained a 1 keV proton beam from a Duo Plasmatron ion source. A water cooled Helmholtz coil provided a 2 kG field and cylindrical trap electrodes were made of conventional 2 3/4 inch conflats and

vacuum pipes. The trap was differentially pumped by an ion pump. The pressure was as good as 2×10^{-8} Torr when the beam was off. However, hydrogen atoms entering the trap with the beam make the pressure worse, partly because neutral atoms are knocked off the walls by the beam. Protons were trapped from a pulse with instantaneous intensity of approximately 4 nA sent through the trap by suddenly raising the potential of the upstream electrode [7]. We held the protons for several milliseconds during which protons oscillated for several thousands of periods, and then quickly lowered the kV potential of the down beam electrode so that trapped protons could escape from the trap towards the channel plate detector. A multiscaler, started when the potential was lowered accumulated a time-of-flight spectrum of pulses from the channel plate. As shown in Fig. 3.1(b), the 1 keV protons trapped from the beam arrive at the detector first and make a distinct peak. Soon after, a low energy proton background begins arriving, followed by heavier background ions. These are from background gas ionized by the incident proton beam.

For a single catch of protons from the beam, approximately 10^2 energetic protons were trapped. The incident beam of 4 nA means that about 10^4 protons were within the trap so that approximately 1% of the available particles were trapped. The low trapping efficiency is due in large part to the low magnetic field and to the large spatial spread in the incident proton beam. This was greatly improved later.

3.2 First capture of antiprotons in an ion trap

As an important step to demonstrate the feasibility of loading and storing antiprotons in the trap, we set up a simple system in LEAR and demonstrated capturing antiprotons in an ion trap [9]. The outline of the trap electrodes, the

scintillator and the magnetic field is Fig. 3.2(a). The slowest antiprotons leaving the degrader are confined in 2 dimensions to field lines of the 6 T superconducting magnet and are so guided through the series of 3 trap electrodes. As the antiprotons enter the trap, a first ring-shaped trap electrode (the entrance endcap) and a main ring electrode are both at 0 volts. A third cylindrical electrode (exit endcap) is at -3 kV so that negative particles with energy less than 3 keV turn around on their magnetic field lines and head back towards the entrance of the trap. Approximately 300 ns later, before the antiprotons can escape through the entrance, the potential of the entrance endcap is suddenly lowered to -3 kV, catching them within the trap. The potential is switched in 20 ns with a krytron circuit developed for this purpose and is applied to the trap electrodes via an unterminated coaxial transmission line [53].

After antiprotons are held for sometime between 1 ms and 10 minutes, the potential of the exit endcap is switched from -3 kV to 0 volts in 20 ns [53], releasing the antiprotons from the trap. The fast releasing of particles allows the most sensitive detection, but results in saturation of the detection system when too many particles are released from the trap. The antiprotons leave the trap along respective magnetic field lines and annihilate at a beam stop well beyond the trap. The high energy charged pions which are released are detected in a 1 cm thick scintillator outside the vacuum system. A multiscaler started when the potential is switched records the number of detected annihilations over the next 6 μs in time bins of 0.4 μs. Time-of-flight spectrum of detected pions from antiproton annihilation is shown in Fig. 3.2(b). The antiprotons were held 100 s in the trap and then released from the trap at time $t = 0$. The spectrum includes 31 events which corresponds to 41 trapped particles when the detector efficiency of 0.75 is included. A second multiscaler records the pion counts over a wider time range with less resolution to monitor backgrounds. These numbers are lower limits since the detection electronics was clearly saturated.

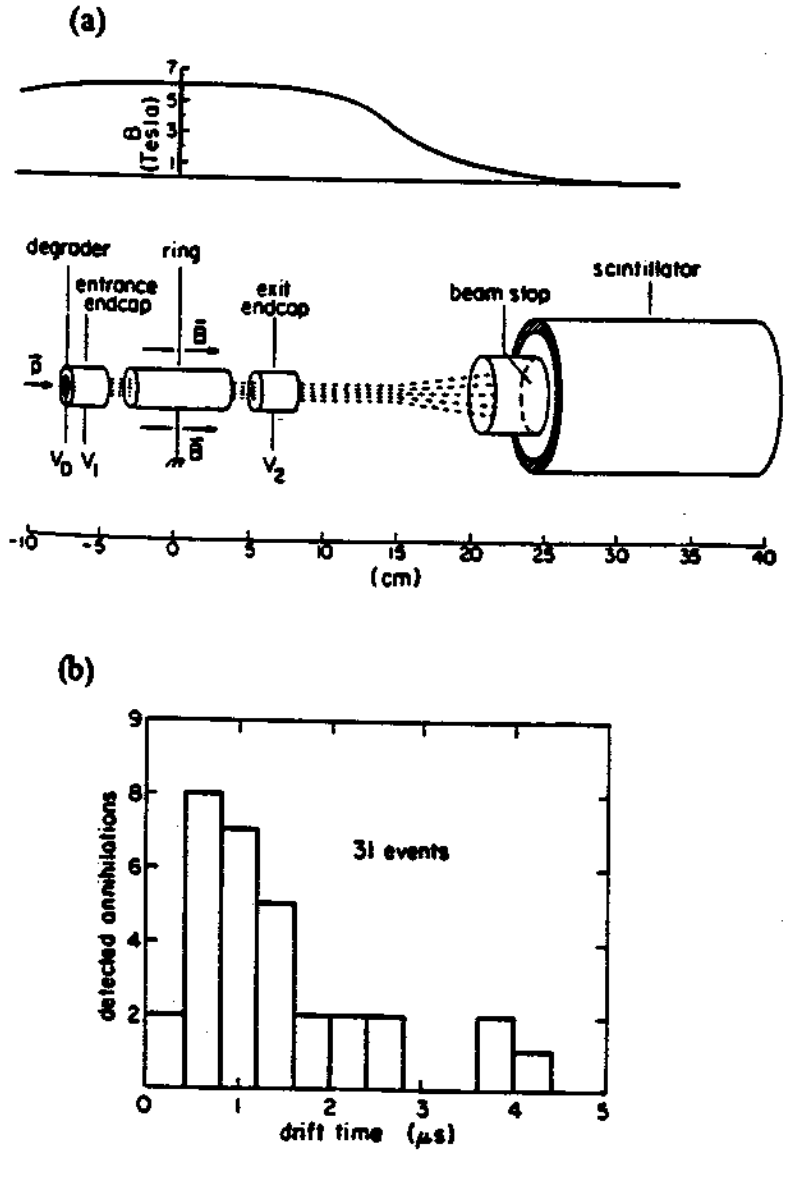

Figure 3.2: (a) Outline of the trap electrodes, the scintillator and the magnetic field. Magnetic field lines are indicated by dashed lines. (b)Time-of-flight spectrum of detected pions from antiproton annihilation.

3.3 Experimental layout for trapping antiprotons in the improved system with a 5.9 MeV antiproton beam

Fig. 3.3 shows the apparatus for trapping antiprotons from LEAR with 5.9 MeV incident energy. It consists of the degrader system described in Chapter 2, a 5.9 Tesla superconducting solenoid, scintillator counters for antiproton annihilation detection, a high vacuum enclosure for the open-end cylindrical trap [54], the cryogenic system for the solenoid, the trap, electronics control for performing experiment, and the data acquisition system.

The 5.9 Tesla **superconducting solenoid** with 10 cm (diameter) bore is made by Nalorac Cryogenics Corporation. The bore can be at room temperature or at 77 K. The solenoid is wound of single strand NbTi wire. Drift rate in the magnetic field is less than 1 part in 10^9/hr. The field homogeneity can be shimmed better than 1 part in 10^8 over a 1 cm diameter sphere. A special configuration of superconducting solenoid winding makes the superconducting system self-shielding against fluctuations in the ambient field [55]. The maximum shielding factor is 156 for a uniform perturbation [56]. There are two cooling reservoirs for the magnet cryostat. The liquid helium dewar volume is 47 liters with a hold time typically more than 3 months. That is a boil-off rate of order 20 ml/hr. The liquid nitrogen main reservoir has a volume of 92 liters. The boil-off rate is less than 200 ml/hr so that the hold time is more than two weeks. The 100 cm bore allows the access of the trap system and housing for detectors and degraders. An auxiliary dewar with a liquid nitrogen reservoir is under the magnet to allow the room temperature bore to be cooled to 77 K.

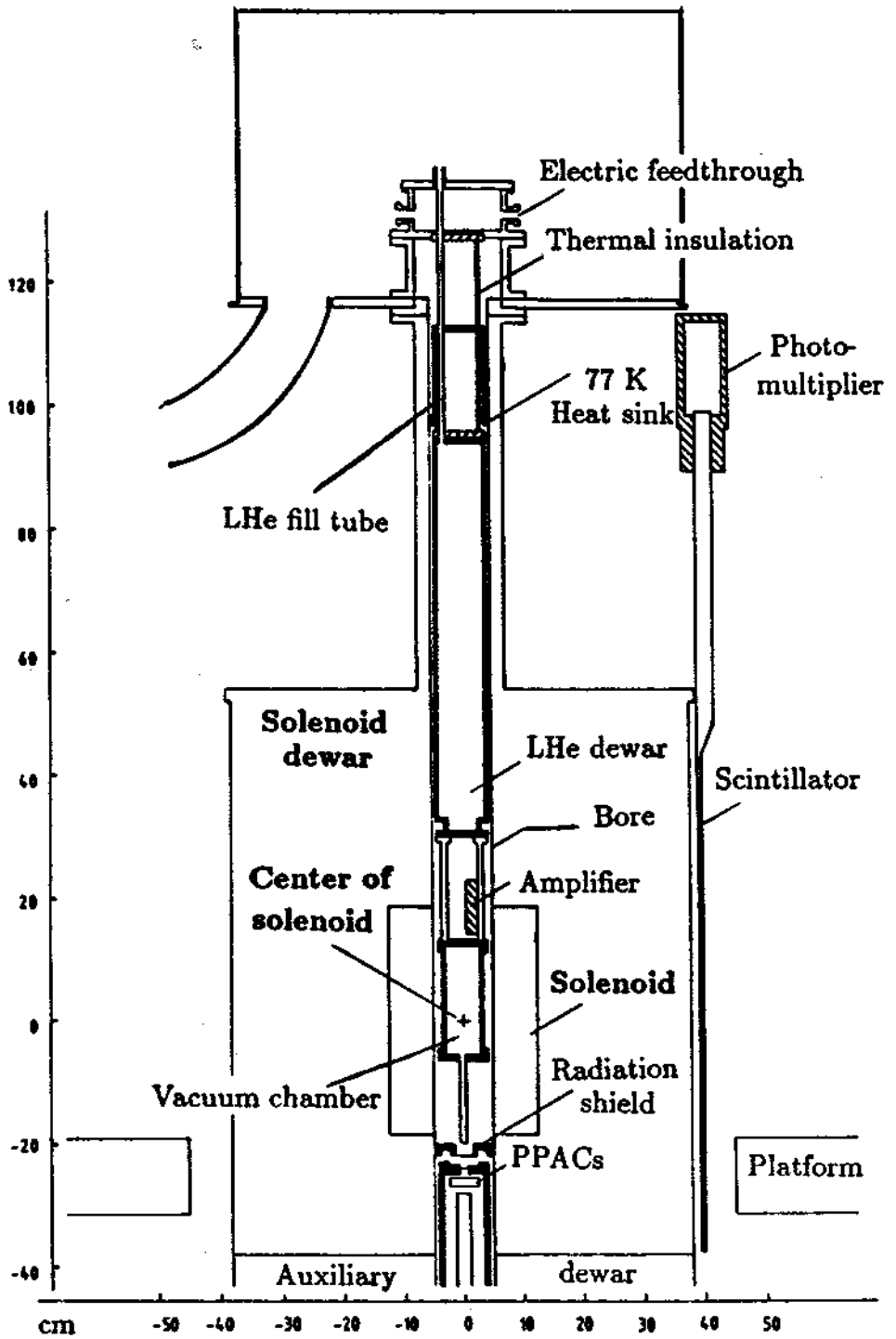

Figure 3.3: The apparatus for the antiproton trapping experiment.

A high vacuum enclosure (trap can) at the center of the solenoid houses the ion trap. A Ti window separates the magnet bore vacuum and the trap can vacuum. Up to 3 amplifiers have been mounted in the space between trap can and the LHe dewar. The amplifier will be described in Chapter 5. The liquid helium dewar has a volume of 4 litres and provides heat sink more than 5 days before a LHe refill is required. Electronic wires and cables exit the vacuum system via electrical feedthrough at the top of the magnet bore.

3.4 Scintillator detectors and the detection efficiency

There are six flat (1 cm thick) plastic scintillators (each with an active area of 0.76 m $\times$ 0.43 m) surrounding the solenoid dewar. The side view of a scintillator is shown in Fig. 3.3. The front view of one scintillator is shown in Fig. 3.4(a). The top view of the configuration of six scintillators is shown in Fig. 3.4(b). Antiproton-proton annihilation produces 2.9 charged pions in average [57]. Light generated by the charged pions go through light guides and hit the photo-cathodes of the photomultipliers (Hamamatsu phototube R2238). The gain is approximately 6×10^6 at a bias potential of +1300 V. The bias potential is off during the intense 300 ns antiproton pulses to protect photomultipliers which otherwise take many seconds to recover. A reed relay described in Chapter 4 turns the potential back on. It reaches 1.3 kV after 0.7 sec, due to the power supply current limit and RC constant in the phototube circuit. The quantity A, defined as the percentage of solid angle subtended to the position in trap axis by scintillators over 4π, as a function of height is shown in Fig. 3.4(c). The solid angle of scintillator coverage to the trap center is A = 70% of 4π and it varies very slow near the trap center. The solid

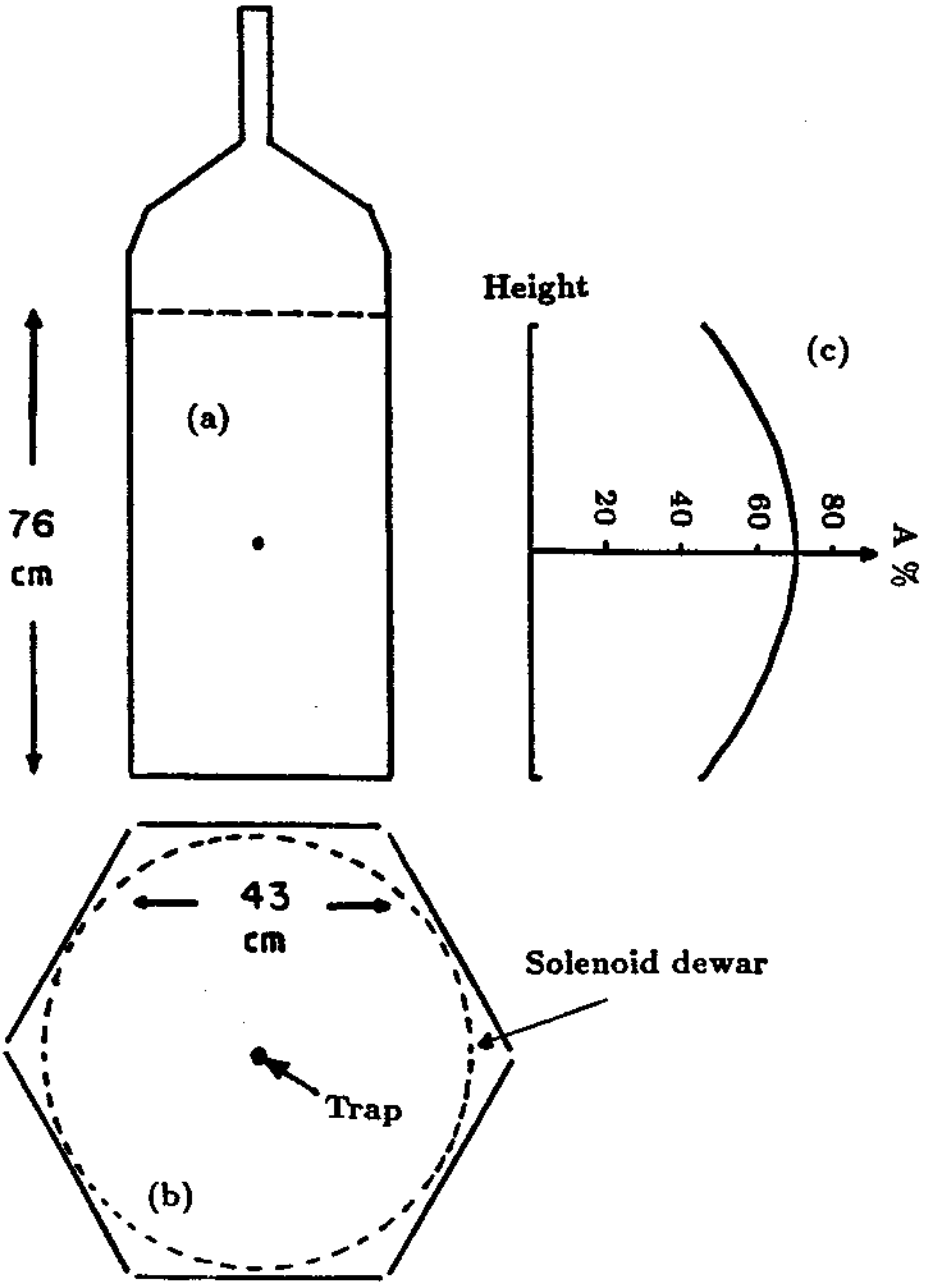

Figure 3.4: (a) Front view of a scintillator. (b) Top view of six scintillators configuration. (c) Solid angle coverage A as a function of height.

angle is only 1% smaller at the point 10 cm away from the trap center along the axial axis.

The detection efficiency of the scintillators is measured in slow extraction mode. For each antiproton coming from LEAR which is detected in the PPAC detectors, we measure the probability that the scintillators detect the annihilation. PPAC counters monitor the incident beam flux. The coincidence signals of PPAC and scintillators in 1 μs time window divided by the PPAC signals gives the efficiency. The efficiency of $70 \pm 2\%$ was measured when the 6 T magnetic field was absent. Correction due to 10% antiprotons struck on molybdenum grid which supports the mylar window in the PPAC detector is about +1.3%. Thus the efficiency is $71 \pm 2\%$ when the magnetic field is off. It is consistent to the pion multiplicity (average of 2.9 charged pions per antiproton annihilation [57]) and the solid angle subtended. Based on the pion decay channels, and the solid angle covered by scintillators, the detection efficiency is estimated to be below 88%. The energy loss of the pions decreases the efficiency to around 80%. The observed efficiency (71%) indicates the photomultipliers and the detection electronics have an average efficiency of 90%.

The magnetic field only has very small effect to relativistic pions. However, the presence of the magnetic field would decrease the gain of the photomultipliers and thus the detection efficiency. In the Fig. 3.5, the coincidence signals of PPAC and scintillators divided by the PPAC, C%, versus the scintillator counting rate are plotted when the 6 T magnetic field is on and off. The detection efficiency of the scintillators is obtained by extrapolating the counting rates to zero. The slopes are due to the antiproton annihilations detected by scitillators but undetected by PPAC since the PPAC has lower detection efficiency at the bias potential used in the experiment, and also due to the background signals from scintillator signals. The efficiency is $46 \pm 3\%$ when the 6 T is on. The correction due to the Mo grid is 0.9%. Therefore, the efficiency for the scintillators detection of an annihilation

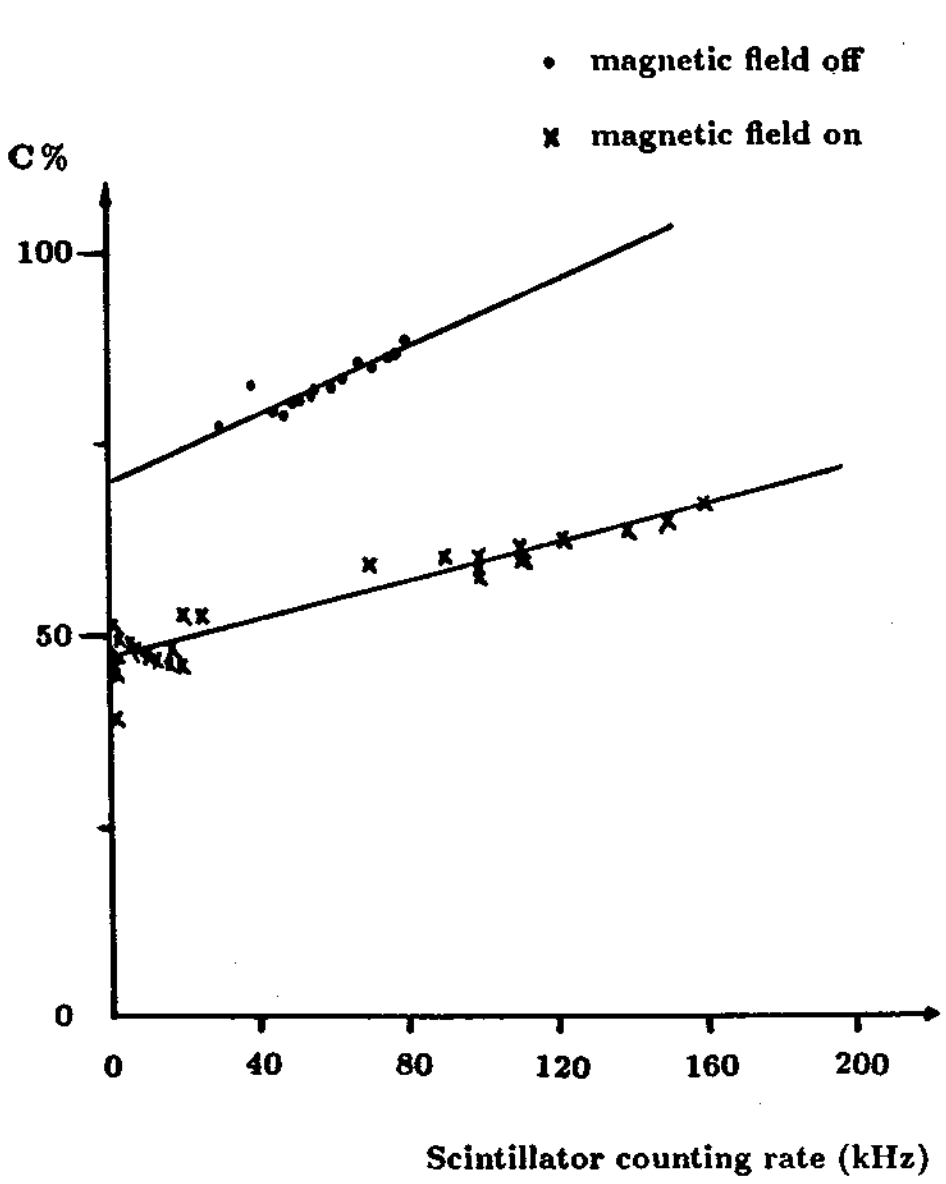

Figure 3.5: Coincidence signals of PPAC and scintillators divided by the PPAC, C%, versus the scintillator counting rate. The scintillator detection efficiency is obtained by extrapolating the counting rates to zero.

event in the trap is measured to be $47 \pm 3\%$.

3.5 Multiple scatterings

As antiprotons pass through a medium they are deflected by many small-angle nuclear elastic scatterings or multiple scatterings. A parallel beam of particles penetrating degrader spreads out into a cone by multiple Coulomb scattering. The distribution of deflection angle θ for particles passing through foils is approximately Gaussian [27]

$$F(\theta)d\Omega = (1/2\pi\theta_0^2)exp[-\theta^2/2\theta_0^2]d\Omega \tag{3.3}$$

with the characteristic angle θ_0. The relative number of particles entering a cone of half angle θ_0 is 39%. As shown in Fig. 3.6, the material that causes the multiple scattering in our trapping experiment is labeled and the angle θ_0 for each layer is indicated. The 5.9 MeV antiprotons penetrating a 10 μm thick Ti foil have $\theta_0 = 0.7°$. The θ_0 for the beam going through the material before the final Al foil (in the trapping experiment, the 117 μm Al foil is moved back about 20 cm) is approximately $2° = 0.035$ radians. The displacement ($L\theta_0$) after particles traveling L = 20 cm is 0.7 cm. Particles hitting the centre of the first Ti foil of the degrader will have a spot size with a diameter of 1.4 cm (which is slightly larger than the trap diameter) on the Al foil with 39% of the beam. This corresponds to a diameter of approximately 0.5 mm at PPAC detectors. In this configuration, the first Ti foil is located very close to the solenoid center so that the scattering due to this foil does not dominate the overall multiple scattering effect. However, if the first Ti foil is 1 m below the final degrader (Al), only about 12 % of particles from the beam could enter the trap without considering scattering effects from other degraders. To minimize the distance, we have our extension of LEAR beamline protrudes up into the bore of the superconducting solenoid as mentioned in Chapter 2.

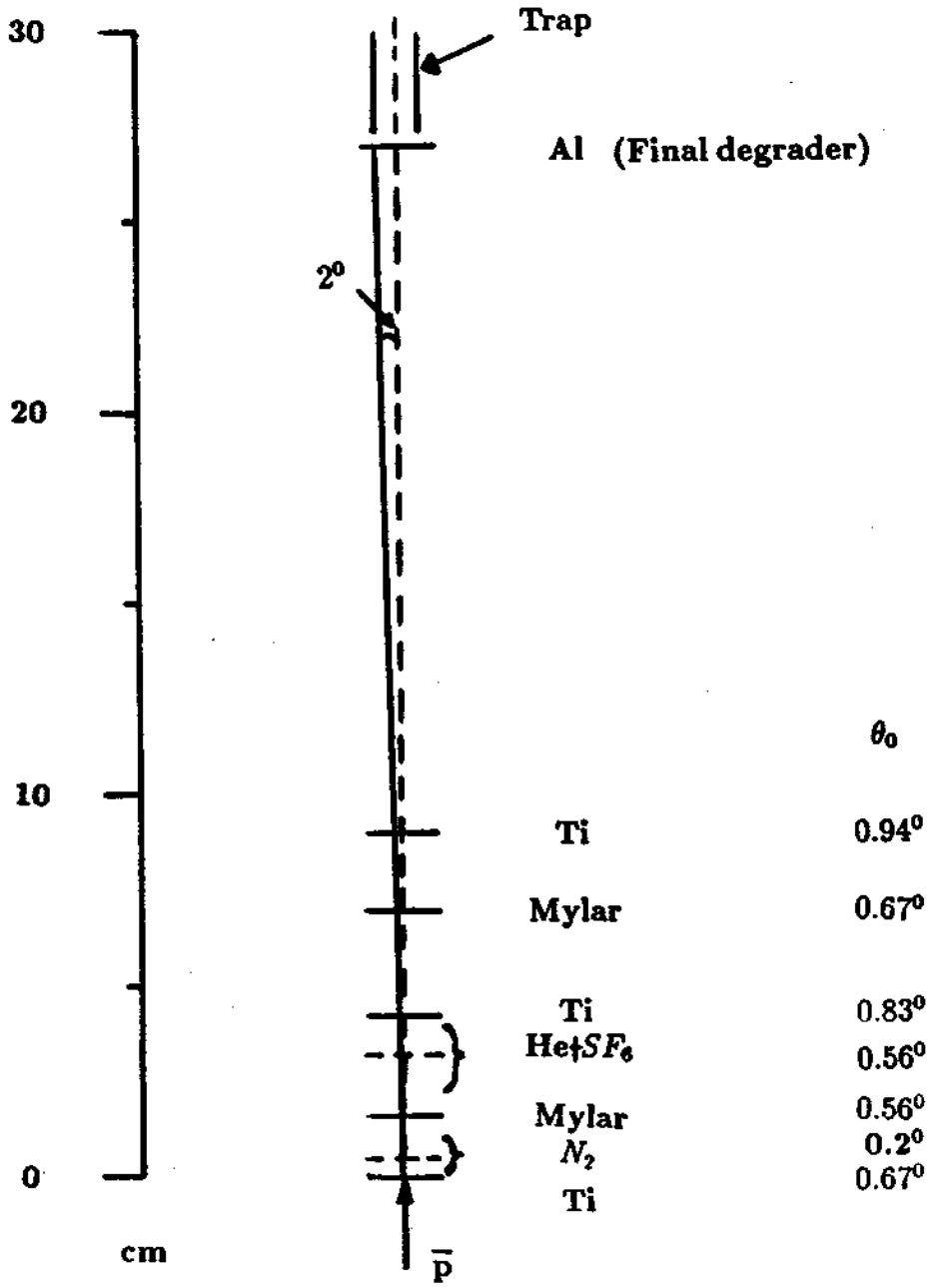

Figure 3.6: Multiple scattering. Each layer is listed in order in Table 2.1 (along with the equivalent thickness of aluminum and the energy loss).

3.6 Electronics

During fast extraction, up to 3×10^8 antiprotons are ejected from LEAR in one pulse with a duration of 300 ns. The potential bias on PPACs is reduced to much lower voltage, typically 100 V, to avoid secondary particles causing sparks. This potential corresponds to a reduced field strength of 13 V/cm/torr. The electrons (and ions) produced by antiprotons in the isobutane gas are proportional to the incident particle numbers, and are collected with the aid of the electric field. Similar to the detection scheme discussed in Chapter 2, signals from 10 channels are amplified by a factor of 10. They are attenuated by a factor of 2 or 20 and fed into an integrating ADC. In Fig. 3.7(a), electronics for one channel of PPACs is shown. A storage scope for one central PPAC channel is used to measure the beam time structure. It will be mentioned again in the timing system. The computer read out from the ADC channels shown in Fig. 3.7(b) shows the beam profile during fast extraction. The higher column in each channel corresponds to an attenuation of 2. The lower one is with 20. The spot size on the PPAC detectors is about 3 mm×3 mm which is mainly due to the beam size. The additional spread due to the multiple scattering is relatively small (0.5 mm) as discussed in Section 3.5.

The **high voltage (HV) ramp** is achieved by using low voltage ramp generator controlling a KEPCO (OPS 5000) high voltage power supply (Fig. 3.8). Resistors are chosen so that a low voltage ramp generator has a linear ramp output voltage from −5 V to 0 V produces a linear high voltage ramp from −3 kV to 0 V. Typically we used a 90 ms ramp for this experiment which is a rate of 31 V/ms. However, this rate can be (and was) easily adjusted to make it up to 100 times faster or 10 times slower. The high voltage ramp output is connected to the exit electrode of the long trap. A resistor divider is used to monitor the HV ramp with a scope. The divided signal is also sent to a waveform digitizer (Lecroy 2256A) and recorded in a computer together with a multiscaler spectrum of the

(a)

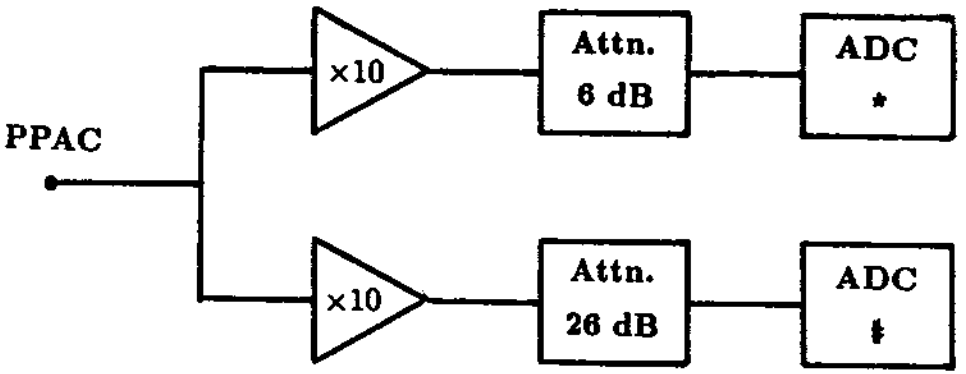

(b)

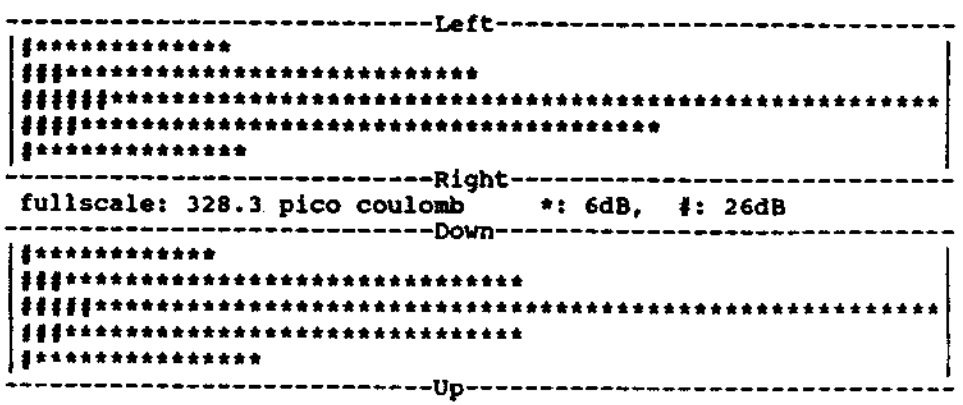

Figure 3.7: (a) Electronics for one channel of the PPACs. Other 9 are identical. (b) Beam profile during fast extraction.

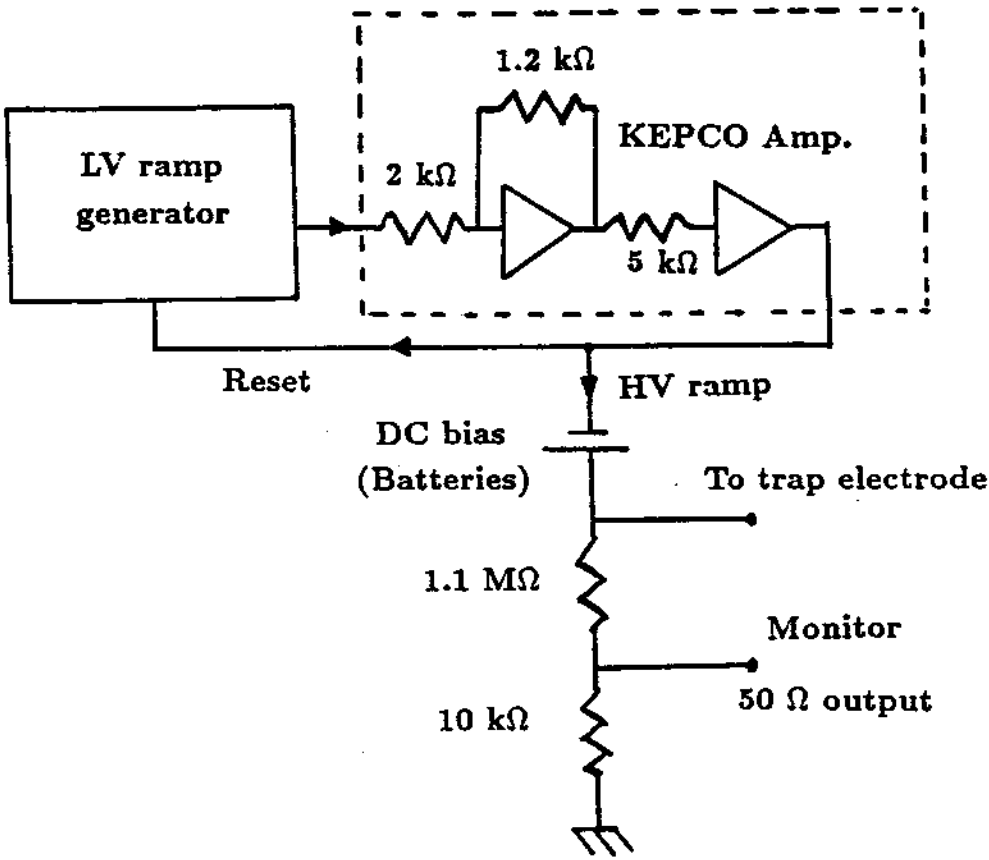

Figure 3.8: Block diagram of the high voltage ramp.

pions from antiprotons which escape the trap as the well depth is lowered.

The timing sequence and block diagram for the timing electronics are shown in Fig. 3.9 and Fig. 3.10. The timing sequence for trapping antiprotons is triggered by a LEAR warning pulse 2 μs before the beam arrives. This warning pulse starts a programmable digital delay/pulse generator (SRS Model DG 535) which has multiple outputs of TTL and NIM signals. One output signal triggers the antiproton load pulser to rapidly apply -3 keV to the degrader to trap particles at a selected time after antiprotons pass through the PPACs. The time difference t_L between the antiproton pulse and the leading edge of the load pulser is measured by a storage scope. The width of the beam pulse (typically 300 ns) reflecting the adjustable LEAR kicker length is also measured by the same scope. The beam profile is recorded by the ADC channels (Fig. 3.7). The exit electrode is at -3 kV potential initially. A potential well for negative particles is formed once the load electrode is switched on. After a preset time (the trapping time or hold time), the function generator sent out a pulse to trigger the HV ramp while at mean time another pulse starts the Joerger multiscaler for counting antiproton annihilations when particles leak out the trap because the well depth is reduced by the ramp.

3.7 Experimental results of trapping study of incident 5.9 MeV antiprotons

In the antiproton trapping experiment, pulses of 5.9 MeV antiprotons leave LEAR beam line upwards through various material (see Table 2.1 and Fig. 3.6) and finally pass through a Ti vacuum window into the trap can, a complete sealed vacuum enclosure which is cooled to 4.2 K. The trap electrodes and the potential

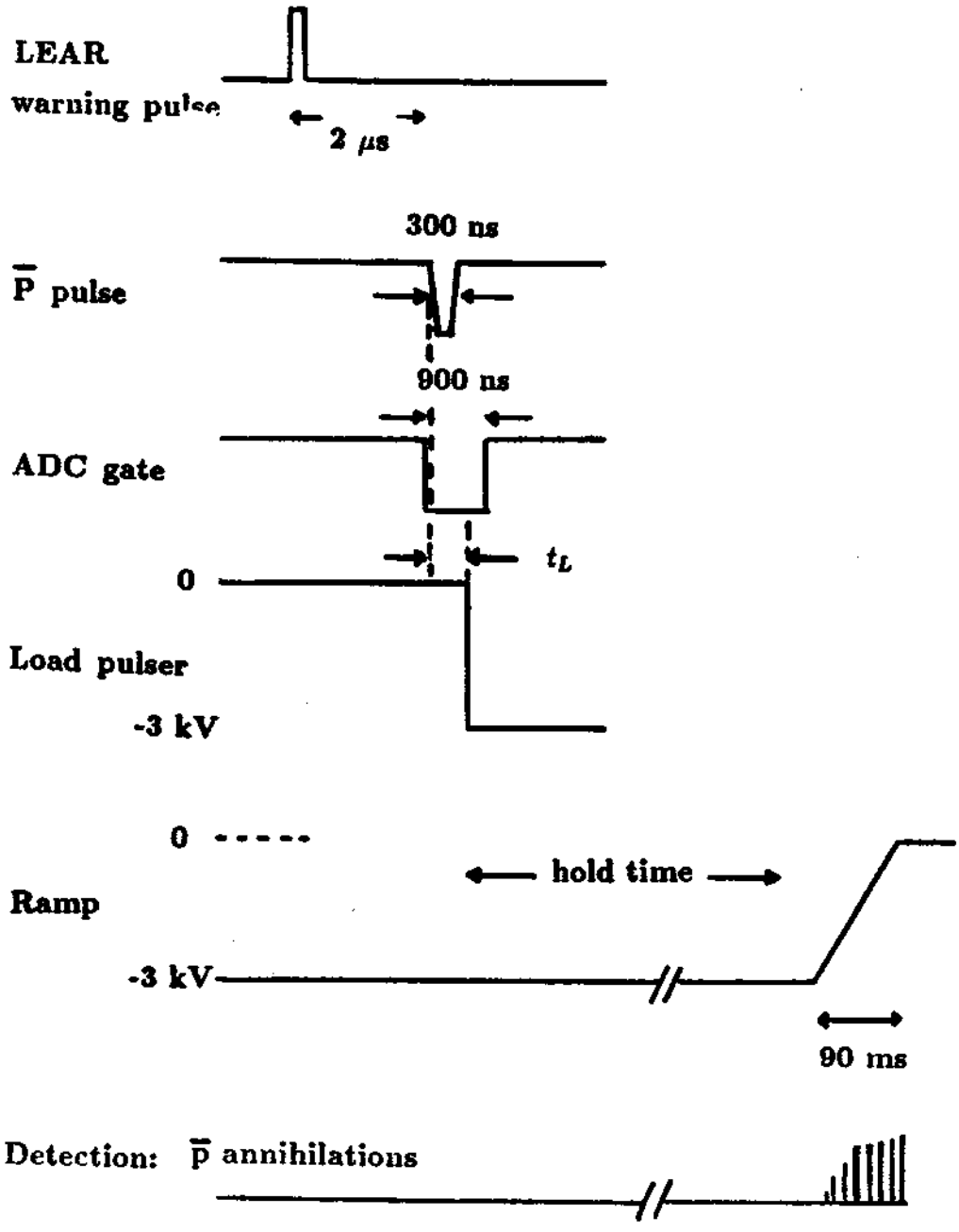

Figure 3.9: Timing sequence from LEAR warning pulse, to LEAR beam detection by PPAC, potential well switching for loading antiprotons, HV ramp to release trapped particles, and particles energy analysis.

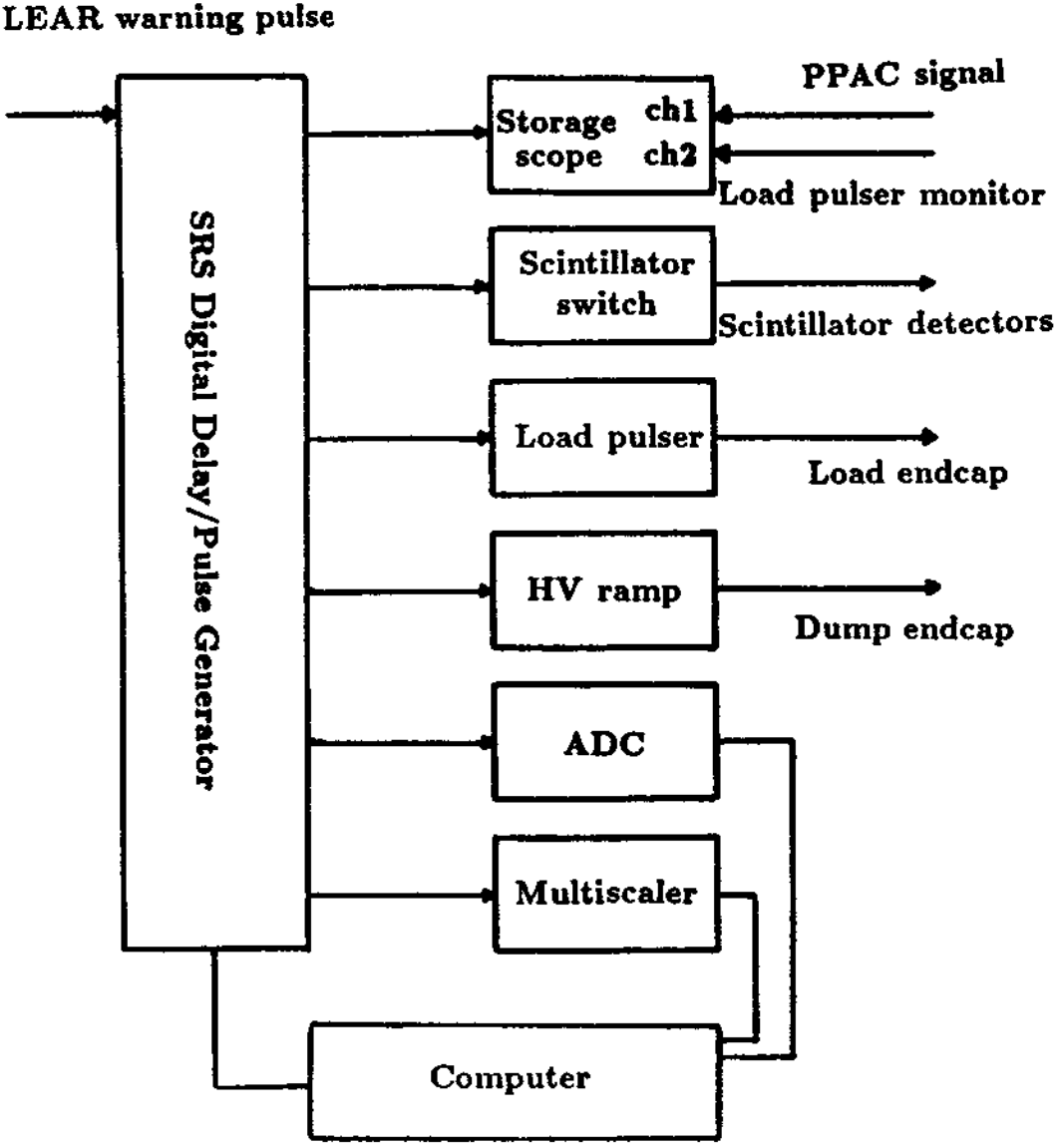

Figure 3.10: Timing block diagram

along the axis of the trap are shown in Fig. 3.11. The ion trap inside consists of an aluminum plate at the bottom which is our load electrode connected with the load pulser, a series of copper cylinders above which can be separately biased to shape the trapping well, and a copper cylinder (or a plate) at the top as our exit electrode attached to the HV ramp. The antiprotons are at approximately 3.7 MeV before they enter the trap by passing through the aluminum plate and their energy can be tuned slightly by adjusting the contents of the gas cells to maximize the number of antiprotons [10] which emerge from this degrader after being slowed below 3 keV, as described in Chapter 2.

Secondary electrons liberated from the degrader by antiprotons are eliminated by biasing the degrader at +5 V or higher with respect to the first cylinder at the bottom. If this is not done, we end up with a trap filled with electrons after the intense antiproton pulse arrives. Similar to the experiments of first capture of protons and antiprotons, the cylinders between load and exit electrodes are grounded (or at a potential much less compared with 3 kV). The upper exit electrode is biased at −3 kV to turn around antiprotons with kinetic energies (along the beam axis) below 3 keV. After the pulse of antiprotons is within the electrodes of the long trap, the potential of the Al degrader is quickly switched to −3 kV, completing the ion trap and confining the particles.

After a preset hold time, the potential of the upper electrode is ramped through 0 V. If the antiproton energy is not too low, the period of the axial oscillation along the magnetic field is very short compared to the 90 ms ramp. For example, oscillation period is about 20 μs for 1 eV antiprotons while the ramp time from −1 V to 0 V is 22 μs. Here the trap length L = 16 cm is used. The oscillation period in the long trap is approximately: t(ns) = 44L(cm)/$\sqrt{E(keV)}$. Therefore almost all the particles in the trap satisfy this condition. Antiprotons with energies exceeding the ramp voltage leak out the trap and their annihilation signals detected

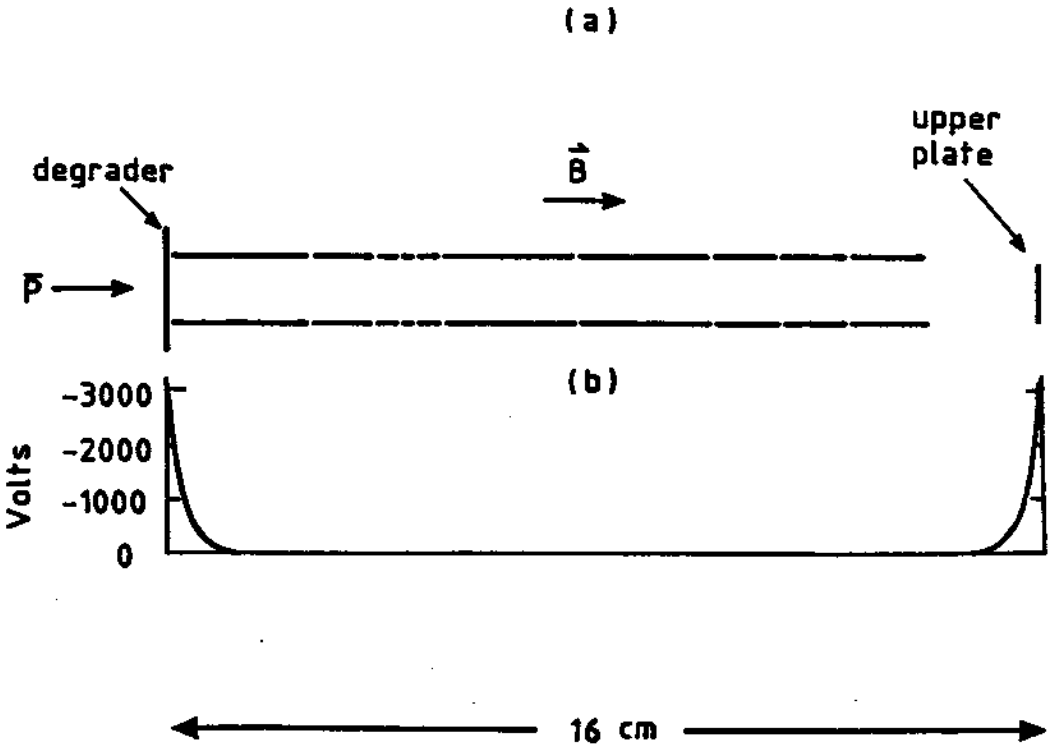

Figure 3.11: (a) Trap electrodes. (b) The potential along the axis of the trap.

by scintillators are recorded in a multiscaler which starts counting when the HV ramp starts. The multiscaler spectrum makes a direct measure of the axial energy.

Fig. 3.12, shows a spectrum of released antiprotons from the long cylindrical trap after being held for 100 sec. Antiproton annihilations are plotted as a function of the high-voltage endcap potential which ramps down with a rate of 31 V/ms. Approximately 6×10^4 counts are detected by scintillators which means about 1.3×10^5 antiprotons had been trapped for 100 sec. The average energy of those antiprotons is 854 eV. The spectrum peaks at low energies and falls off at higher kinetic energies as the antiproton energy approaches the 3 keV well depth. The low energy peak is only present for the most intense bursts of antiprotons from LEAR. It seems to be due to electron cooling by secondary electrons liberated from the degrader when the most intense pulses of antiprotons from LEAR hit it. Approximately 500 counts in one single channel at low energy peak which corresponds to an average energy distribution of 1 annihilation count for every 10 meV energy window. Here we used the energy resolution of 6.1 V/channel. Even when we just count the flat part of the spectrum, there are 200 counts or 400 antiprotons/channel. Then the average particle distribution is 1 antiproton per 15 meV.

The scintillator detection shows that the double hits (when two scintillators detecting the same antiproton annihilation event) to single hit ratio is 0.36 which was reproducibly measured. Using the number of antiprotons measured to leave LEAR (3×10^8), we trap antiprotons from LEAR with an efficiency of 4×10^{-4} or 1.4×10^{-4}/keV. It is very close to our degrader test result of 1.6×10^{-4}/keV which is a lower limit of the antiproton yield. Trapping efficiency can vary a lot depending on LEAR beam tuning (such as beam focusing and steering, pulse width, shape and timing), and our experimental setting (such as the amount of degrader and the quality of the degrader, and load timing). Less trapped antiprotons by a factor

of 10 is more typical when the LEAR beam is not optimally tuned.

The number of antiprotons with axial energies less than 3 keV captured in the long trap, normalized to the number of antiprotons in the pulse (PPAC signals) from which these were trapped, is plotted as a function of the gas mixture (Fig. 3.13). The hold time for each trial (represented by a point in the plot) was 10 sec. The width (FWHM) of the curve is equivalent to 33% of SF_6 change in gas cell 2. In energy it is 0.17 MeV (or 12 μm in Al thickness) which is 23% of the total degrader tuning range by gas cells. The gas mixture corresponding to maximum trapping efficiency is reproducible.

With the gas mixture optimized and an antiproton hold time of 10 sec, we plot the trapping efficiency versus the time between when the antiproton pulse enters the trap and the high-voltage potential is switched on by the load pulser Fig. 3.14. The time structure of the antiproton pulse is shown in Fig. 3.14(a). The flat top is 200 ns. The width is typically 300 ns with a 100 ns rise time. An arrow marks the beam entering trap. Relative trapping efficiency versus the load pulser timing t_L (see also Fig. 3.9) is plotted in Fig. 3.14(b). When the potential is switched on too early and most antiprotons are not in the trap yet, the trapping efficiency is very low. As we delay the load pulser trigger to allow more particles to enter the trap, trapping efficiency rises rapidly. As expected, a peak appears right after the whole pulse of beam entered the trap. If the high-voltage switching time is further delayed, particles with higher energy turned around by -3 kV at the upper electrode have time to hit the degrader, causing the drop of the efficiency to the right. For a 16 cm long trap, the period is 430 ns for 3 keV antiprotons, and it is 730 ns for 1 keV particles. Particles with lower energy will take longer time in the trap so that the trapping efficiency is not critically dependent upon the timing.

In one trial, antiprotons were captured and held in the long cylindrical trap for

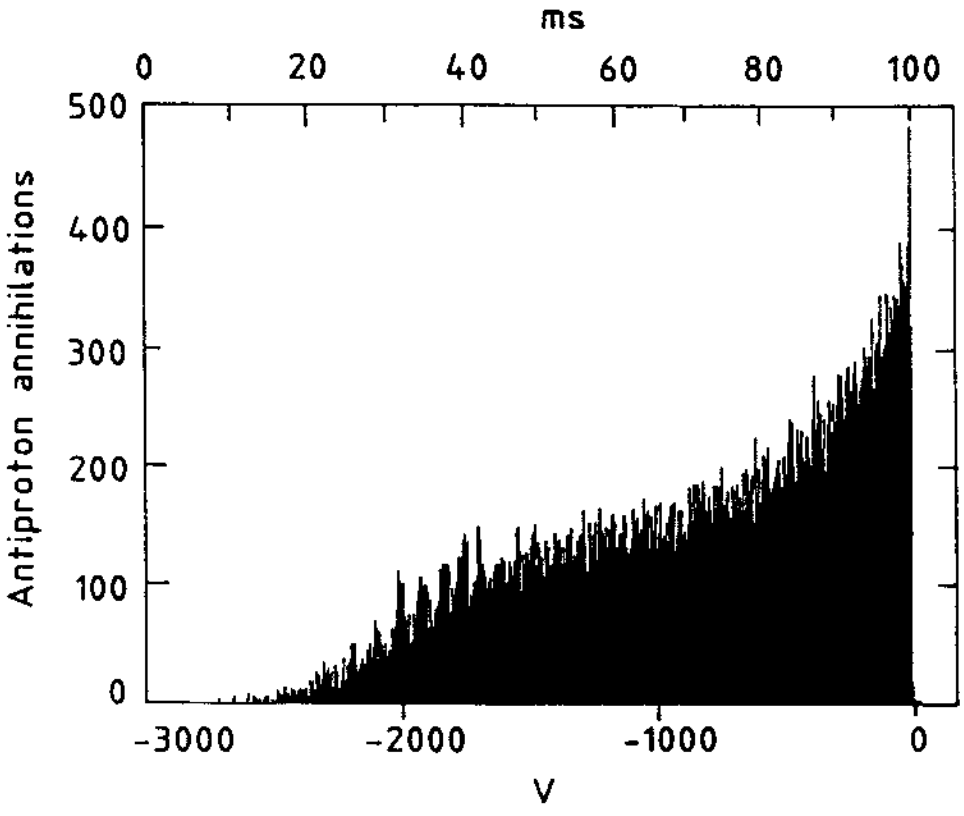

Figure 3.12: Spectrum of released antiprotons from long cylindrical trap after bei held for 100 sec.

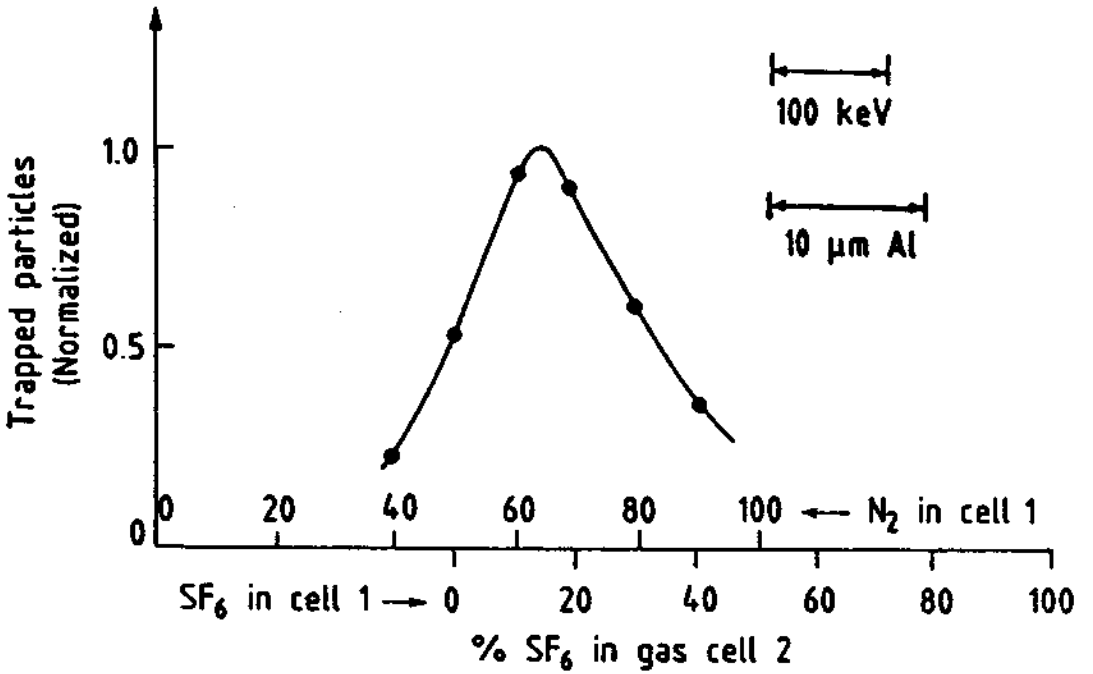

Figure 3.13: Trapping efficiency versus degrader thickness.

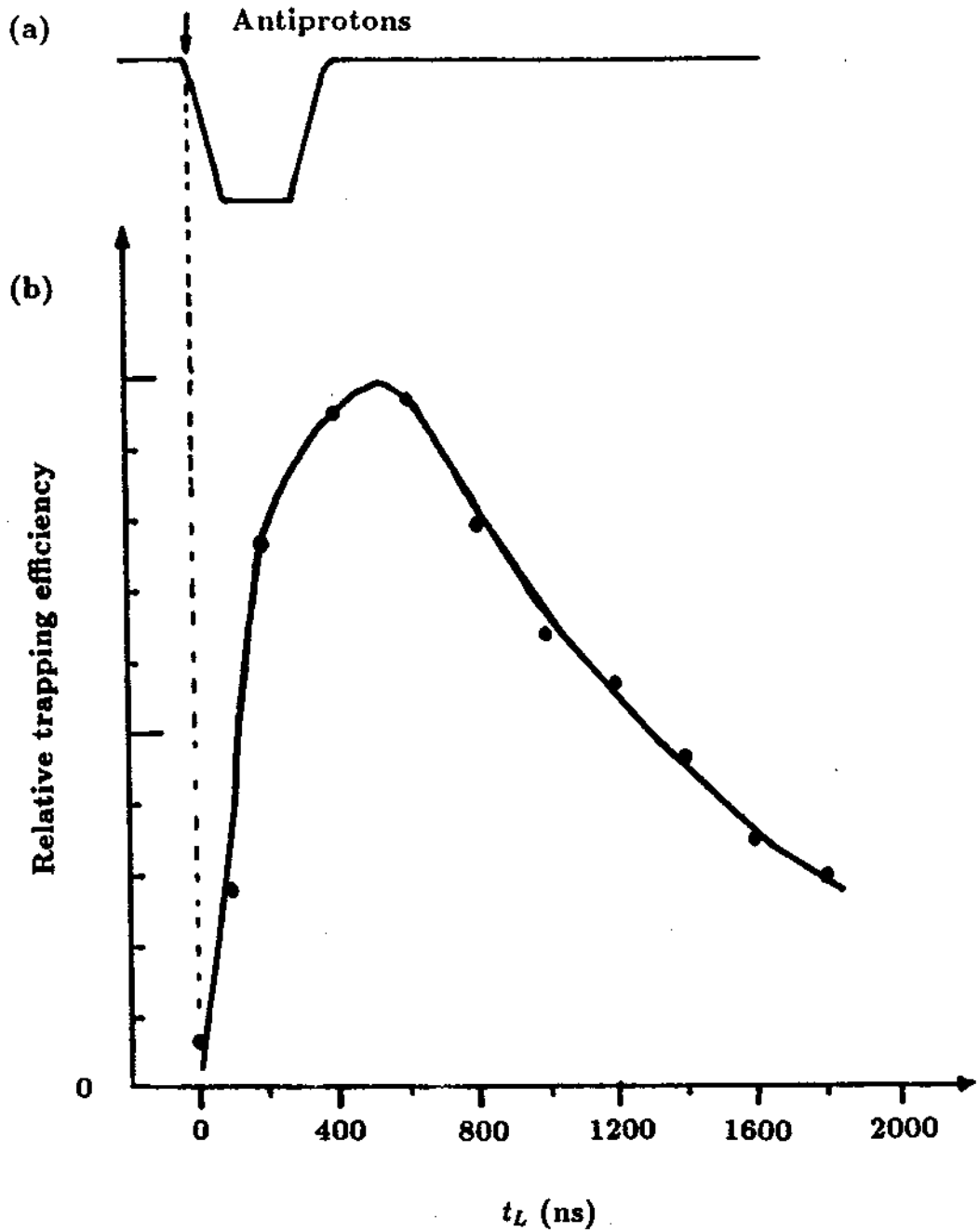

Figure 3.14: Trapping efficiency versus load pulser timing.

64 hours (2.7 days). There were 3933 annihilation counts (representing 8368 antiprotons) recorded in the spectrum (Fig. 3.15). Based on the PPAC signal for this trial and the calibration of trapped antiprotons per unit PPAC signal, we estimate the initial number of trapped particles are less than 2.8×10^4. Thus a lifetime in the long trap of greater than 54 hours is established if we assume that the particles decay exponentially. The average energy of the particles is 0.8 keV, similar to the energy spectrum after shorter hold time.

Although the energetic antiprotons initially loaded into the long trap remained for days, the containment time for low energy antiprotons was significantly shorter. Within several hundred seconds low energy antiprotons were already lost from the long trap. The lifetime for approximately 10^7 electrons in the long trap was measured to be only 5 to 10 seconds, though much longer storage times were observed for shorter sections. One might expect that a long cylindrical trap would be unstable for low energy particles as the potentials applied to the end plates are exponentially screened from the interior, leaving only a homogeneous magnetic field inside. Since no preferred axis is indicated, the particles can be moved across the field lines by stray potentials within the electrodes. An electron storage time inversely proportional to the length squared for similar traps has been observed in plasma physics experiments [58]. This functional dependence has not been explained, but the proportionality constant increased when stray potentials were minimized and axial symmetry was maximized. Our observed lifetime also decreases with trap length. The containment time for low energy particles are greatly improved when we use gold plated short electrodes to produce a high quality electric quadrupole potential (see Chapter 5 and Chapter 6).

We have demonstrated that up to 1.3×10^5 antiprotons from a single LEAR pulse were stored in the ion trap. The trapping efficiency is more than 4×10^{-4}. The kinetic energies of trapped antiprotons are between 0 eV to 3 keV. Further

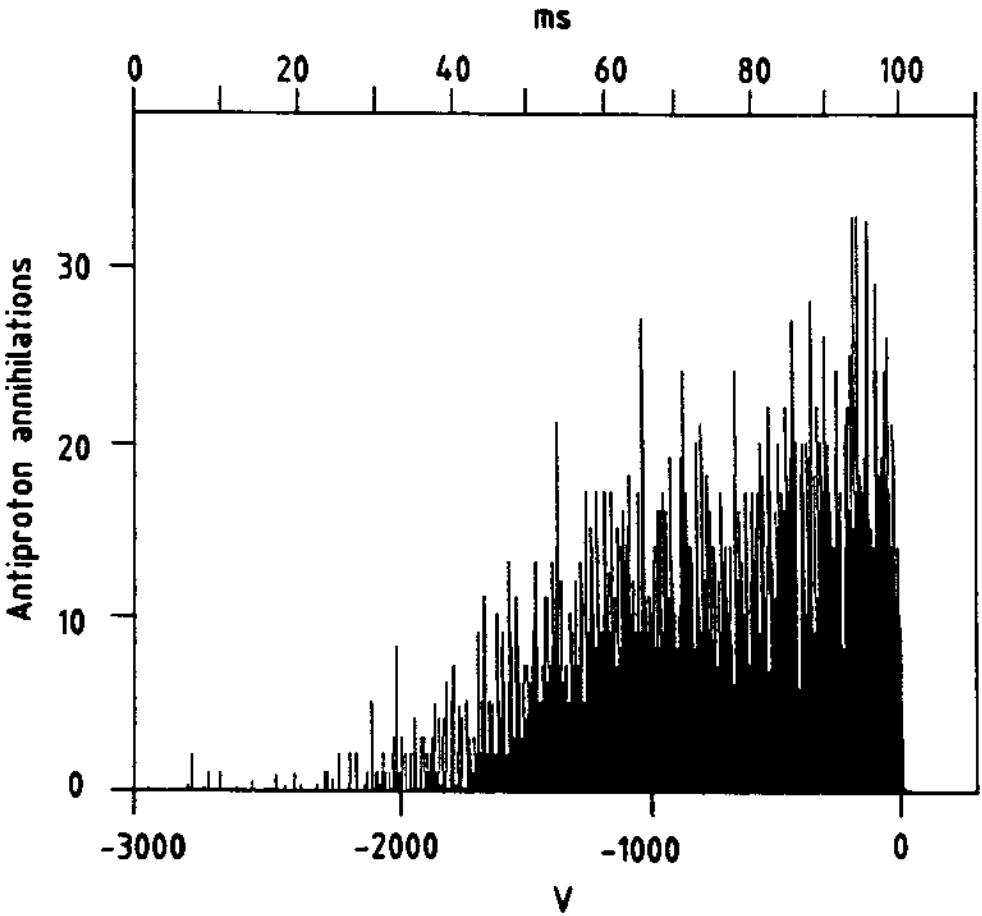

Figure 3.15: Spectrum after holding antiprotons for 64 hours in the long trap

slowing and cooling are realized by collisions between electrons and antiprotons within the ion trap. This will be discussed in Chapter 5 where the width of the energy spectrum is squeezed and narrowed drastically.